

Image edge-enhancement in optical microscopy with a phase mismatched spiral phase plate

Shibiao Wei (魏仕彪)¹, Jing Bu (步 敬)¹, Siwei Zhu (朱思伟)², and Xiacong Yuan (袁小聪)^{1*}

¹*Institute of Modern Optics, Key Laboratory of Optoelectronic Information Science and Technology, Ministry of Education of China, Nankai University, Tianjin 300071, China*

²*Nankai University Affiliated Hospital, Tianjin 300121, China*

*Corresponding author: xcyuan@nankai.edu.cn

Received September 20, 2010; accepted November 6, 2010; posted online February 21, 2011

We present a spiral phase filtering system with a large tolerance for edge enhancement of both phase and amplitude objects in optical microscopy. The method is based on a Fourier 4- f spatial filtering system. A phase mismatched spiral phase plate (SPP) fabricated by electron beam lithography is employed as the radial Hilbert transform for image edge enhancement. Compared with holography, SPP is simple, economical, reliable, and easy to integrate.

OCIS codes: 100.2980, 050.1970, 050.4865.

doi: 10.3788/COL201109.031001.

Biological samples are usually considered as phase-only objects. Therefore, they show only small contrast in conventional bright-field microscopy. In a few recent articles, it has been suggested that coherent spatial image filtering with a spiral phase element leads to a strong edge contrast enhancement of both amplitude^[1–3] and phase objects^[4–7]. Spiral phase filtering is not sensitive to the absolute phase/amplitude of a sample, but to the phase/amplitude gradients that are strongly amplified by redistribution of the image intensity. In contrast, methods like dark-field also use Fourier filters, but lose some image intensity by being partially absorptive. The differential interference contrast (DIC) method is also sensitive to a phase/amplitude gradient; however, it needs to manipulate the polarization of the image wave. The spiral phase element used in Fourier filtering can be a spiral phase plate (SPP) or a hologram displayed in spatial light modulator (SLM). The SPP is a simple, economical, and reliable micro-optical element that can easily be integrated in existing optical systems. In contrast, the cost of using a hologram in SLM is high; moreover, the holograms usually have lower power efficiency than the SPP. A previous study has used an SLM in a microscope to demonstrate the optical edge enhancement image processing^[4], while another work has implemented the isotropic edge enhancement of relief-like images^[8]. Yuan *et al.* have demonstrated an experiment to obtain surface topography of a sample through a self-referenced spiral interference based on a phase-only hollow spiral phase plate^[9]. Situ *et al.* used a spatially incoherent light-emitting diode (LED) with a 1-nm bandwidth filter in the Kohler illumination as the light source, and they demonstrated that using an off-axial holograph could transform the phase specimen into a relief-like view even under such illumination^[10].

In this letter, we demonstrate that coherent spatial image filtering by an SPP has a large tolerance of phase modulation mismatch in terms of fabrication error and/or incident working wavelength. This is done by Fourier spiral phase filters using a phase mismatched SPP (MSPP) that has been designed and fabricated in

house. The results show that this Fourier filtering system can adapt the MSPP with an offset to the incident wavelength, giving rise to broadband light sources in potential applications in the system.

SPP with an azimuthal phase structure of $\exp(i\theta)$ can be employed to implement the radial Hilbert transform. It is a refractive-type element fabricated in transparent material and its diffraction efficiency is close to 100%. The SPP with a unit topological charge has a transmission function expressed as

$$H(r, \theta) = \text{circ}\left(\frac{r}{R}\right) \exp(i\theta), \quad (1)$$

where (r, θ) are the polar coordinates in the SPP plane, $\text{circ}(r/R)$ is the circular aperture function describing the sharp aperture of the SPP with the radius of R . The phase structure of a conventional SPP with a unit topological charge is shown in Fig. 1.

The maximum height h is given by $h = \lambda/(n - n_0)$, where λ is the wavelength, n is the refractive index, and n_0 is the refractive index of the surrounding medium. Ideally, the phase values of the SPP should increase linearly and continuously; however, due to fabrication restrictions, the phase values are quantized to 32 steps in our case. The height h of a static SPP designed for a specific wavelength is not changed. This cannot be satisfied accurately for other wavelengths in optical edge enhancement filtering. In reality, the height of SPP is also

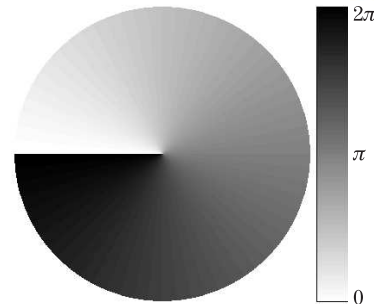


Fig. 1. SPP grey-scale phase plate with a unit topological charge.

usually mismatched due to fabrication errors. Hence, in order to obtain an accurate SPP for a specific wavelength, we have to fabricate many SPPs. In this letter, we demonstrate that the SPP filtering system has a large tolerance for the height mismatch. In our experiment, the SPP was fabricated by direct electron-beam lithography in SU-8 2005 negative photo-resist material with a refractive index of about 1.59. For the working wavelength at 532 nm, the SPP must be designed with the maximum height close to 901.7 nm, which corresponds to 2π -phase difference. Due to fabrication errors, the actual maximum height is only 823.3 nm, that is, the actual maximum height could only produce the 2π phase difference when the wavelength of 485.7 nm is employed. The 46.3 nm offset between the incident light source wavelength and the coincident incident light wavelength of SPP is about 9.5% offset to SPP, which is approximately equivalent to a topological charge of 0.9. Figures 2(a)–(c) shows the simulation results for an optical vortex intensity distribution that are generated by spiral phase plates with different topological charges 1, 0.9, and 0.8 in the Fourier plane, respectively. The other calculation parameters are the wavelength of $\lambda = 532$ nm, Fourier transform lens focal length of $f = 500$ mm, and the radius of the SPP of $R = 3$ mm.

In Fig. 2(a), the field is exactly circular symmetric. Numerical results show that the circular symmetry of the field is broken down if the topological charge is decreased to 0.9 [Fig. 2(b)] and 0.8 [Fig. 2(c)]. When the topological charge becomes a fraction, the diffracted field undergoes a phase discontinuity in the phase along the azimuthal θ . As a result, interference between the diffracted field of the singularity at origin, along with the edge phase discontinuity, breaks the symmetry of the vortex field^[11]. In Fig. 2(c), the SPP topological charge is equal to 0.8, and the asymmetry of the field shows a relation between this asymmetry and the SPP phase distribution. In Fig. 2(b), the SPP topological charge is equal to 0.9 and the field is similar to Fig. 2(a), making it difficult to distinguish between the two. The SPP with the actual maximum height of 823.3 nm and approximate topological charge of 0.9 can perform spiral phase filtering similar to the SPP, in which the maximum

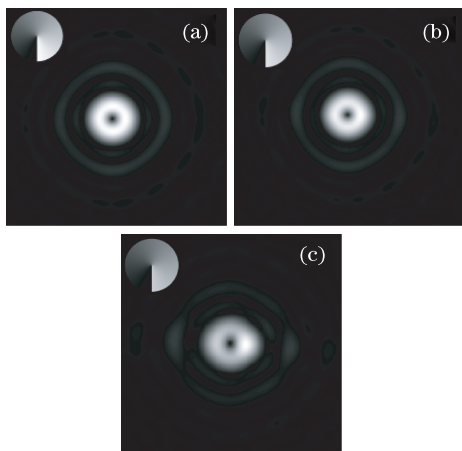


Fig. 2. Simulation for the optical vortex intensity distribution in the Fourier plane with different topological charges: (a)1, (b)0.9, and (c)0.8.

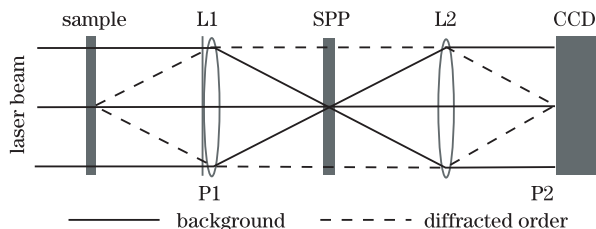


Fig. 3. 4- f system for spiral phase filtering.

height corresponding to 2π -phase difference at the wavelength of 532 nm.

A 4- f Fourier transform-based spiral phase filtering system is shown in Fig. 3, in which the image edge enhancement is formed at the charge-coupled device (CCD) detector. A plane wave is used to illuminate the input pattern $g(x, y)$ placed at the front focal plane of L1 as P₁. In the back focal plane, we obtain the Fourier transform as

$$G(\xi, \eta) = F[g(x, y)], \quad (2)$$

where $F[\bullet]$ is the Fourier transform, and (ξ, η) are the coordinates at the back focal plane.

Thus, we can write the field after the SPP as

$$T(\rho, \theta) = G(\rho, \theta) \cdot H(\rho, \theta) = F[g(x, y)] \cdot H(\rho, \theta), \quad (3)$$

where $\xi = \rho \cos \theta$, and $\eta = \rho \sin \theta$. In a 4- f system, L2 also performs Fourier transform. At its rear focal plane P2, we can obtain the output image field as

$$\begin{aligned} t(r, \phi) &= F[T(\rho, \theta)] = g(r, \phi) \otimes F[H(\rho, \theta)] \\ &= g(r, \phi) \otimes h(r, \phi), \end{aligned} \quad (4)$$

where (r, ϕ) represent the polar coordinates in the CCD plane, respectively; $x = r \cos \phi$; $y = r \sin \phi$; the symbol \otimes represents the convolution operation. $h(r, \phi)$ is referred to as the point spread function (PSF) of the imaging system for radial Hilbert transform with SPP given by^[1]

$$h(r, \theta) = xJ_0(x) + \frac{\pi x}{2}[H_0(x)J_1(x) - H_1(x)J_0(x)], \quad (5)$$

Where, $x = 2\pi rR/\lambda f$, λ is the wavelength of the illuminate light, and f is the focal length of the Fourier transform lens. In addition, J_0 and J_1 are the Bessel functions of the zero and first orders, respectively, while H_0 and H_1 are the Struve functions of the zero and first orders, respectively.

The numerical simulation of edge enhancement was performed by fast Fourier transforming the circular amplitude object, multiplying this pixel by pixel with the respective filter function shown in Eq. (5), and then performing the reverse Fourier transform (Fig. 4). Figure 4(a) shows the original circular image. In Fig. 4(c), the horizontal linear intensity distribution profile of the output Fig. 4(b) shows a strong edge enhancement at the wavelength of 532 nm with an SPP filtering at this wavelength. Figure 4(d) shows the spiral phase filtering result image using an MSPP, which is tailored for an imaging wavelength of 633 nm and an incident wavelength of 532 nm. Figure 4(e) displays the horizontal linear intensity distribution profile of Fig. 4(d). It turns out that the spiral phase plate filtering, whose maximum height with a small offset from the incident wavelength, also

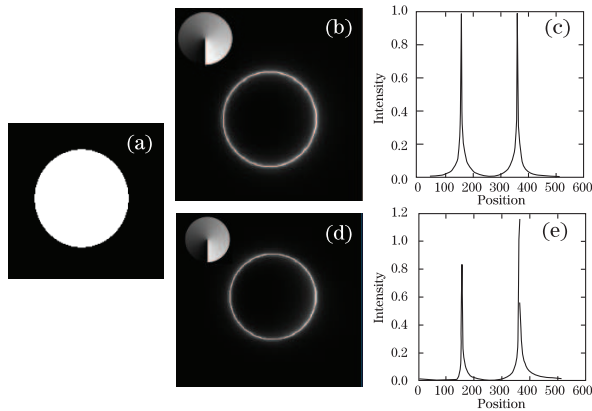


Fig. 4. Simulation of the imaging of a circular input object for the spiral phase filtering method: (a) the input circular object; (b) the simulation result for spiral phase filtering with a matched SPP; (d) the result for spiral phase filtering with a MSPP, which has a small offset from the incident wavelength. (c) and (e) are the horizontal linear intensity distribution profiles of (b) and (d), respectively.

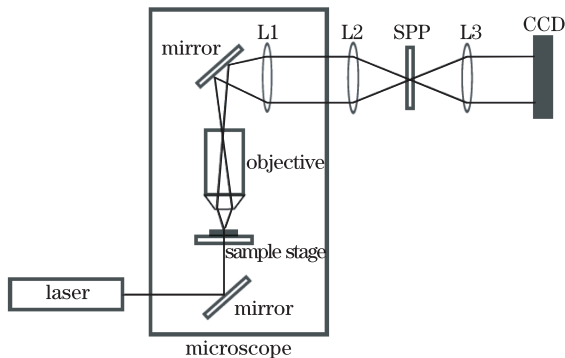


Fig. 5. Experimental setup for optical edge enhancement.

performs a strong edge enhancement for the input sample. However, the intensity of enhanced edge is not perfectly uniformly distribution.

A sketch of a modified optical microscope is displayed in Fig. 5. A sample is illuminated with an expanded laser beam of 532-nm wavelength. After going through the sample, the laser beam was collected by an objective (magnification 40 \times , numerical aperture (NA) = 0.65). A further set of 4- f system for spiral phase filtering is arranged.

The SPP with a radius r of 2 mm was placed at the Fourier filtering plane to perform the spiral phase filtering. The focal lengths of L1, L2, and L3 were 10, 20, and 20 cm, respectively. Here, the image was formed at the CCD detector.

We have chosen living human lung adenocarcinoma cells and onion skin cells for the edge enhancement experiment, and the results are shown in Figs. 6 and 7, respectively. The living human lung adenocarcinoma cells are weak phase objects with a diameter of about 10 μm ; it is difficult to distinguish the cells using conventional bright-field microscope. Figure 6(a) displays the image of human lung adenocarcinoma cells when the 4- f system is removed; in the ellipse region, we almost cannot recognize the cell edges from the culture fluid. Meanwhile, Fig. 6(b) shows edge enhancement using MSPP.

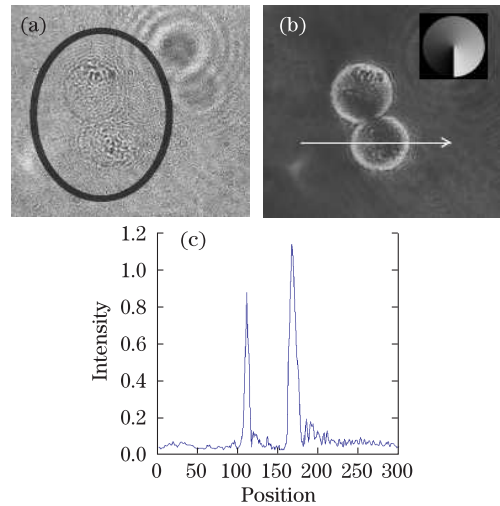


Fig. 6. Edge contrast enhancement of phase objects: (a) image of living human lung adenocarcinoma cells in conventional microscope condition; (b) image of the same cells under fractional spiral phase filtering for edge contrast enhancement; (c) image of the intensity section distribution of (b) in a horizontal direction across the cell of the arrows.

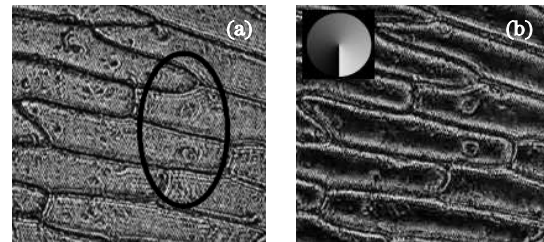


Fig. 7. Edge contrast enhancement of absorptive objects: image of the onion skin cells (a) in conventional microscope condition, and (b) the image under fractional spiral phase filtering for edge contrast enhancement.

Comparing Fig. 6(a) with Fig. 6(b), the cell edges can easily be recognized and the background is also suppressed in the latter. There is a slight light leakage in the inclined orientations. Figure 6(c) shows the intensity section distribution of Fig. 6(b) in the horizontal direction across the cell of the arrows. It shows the asymmetry of the image edge enhancement using MSPP, but the effect is so small that the edges of the cells can still easily be distinguished in a fairly uniform manner. This means that high-contrast edge enhancement is achievable using MSPP for spiral phase filtering.

Figure 7(a) shows the profile of the onion skin cells in the conventional microscope with a 10 \times objective. As an absorptive object, these cells can be distinguished easily, although small details are difficult to distinguish. In Fig. 7(a) the nuclei with a diameter of about 4 μm in the highlighted ellipse region are not clearly imaged. Comparing Fig. 7(b) with Fig. 7(a), both cell edge details and nuclei details are easily distinguished. In terms of edge enhancement imaging, the MSPP filtering greatly improves the resolution of the absorptive objects.

In conclusion, we experimentally demonstrate a simple, reliable, and economical technique for optical edge enhancement. The micro-fabricated MSPP is used for the 4- f system spiral phase filtering. The SPP can be integrated conveniently into the microscope for optical edge enhancement at a low cost. Furthermore, we

demonstrate that the Fourier filtering system has a large tolerance for both phase and amplitude objects in spiral phase filtering. The system can adapt the MSPP with an offset from the incident wavelength. Benefiting from the tolerance, the method can work well for a broadband light source once an SPP is engineered.

This work was partially supported by the National Natural Science Foundation of China (No. 60778045) and the Ministry of Science and Technology of China (No. 2009DFA52300 for China-Singapore collaborations). The fabrication work was partially supported by the Ministry of Science and Technology of China (No. 2010CB327702). The authors would like to thank Dr Jun Chen for his helpful discussions and assistance in this work.

References

1. J. A. Davis, D. E. McNamara, D. M. Cottrell, and J. Campos, *Opt. Lett.* **25**, 99 (2000).
2. S. Bernet, A. Jesacher, S. Fürhapter, C. Maurer, and M. Ritsch-Marte, *Opt. Express* **14**, 3792 (2006).
3. C.-S. Guo, Y. Han, J. Xu, and J. Ding, *Opt. Lett.* **31**, 1394 (2006).
4. S. Bernet, A. Jesacher, S. Fürhapter, C. Maurer, and M. Ritsch-Marte, *Opt. Express* **14**, 3792 (2006).
5. C. Maurer, A. Jesacher, S. Fürhapter, S. Bernet, and M. Ritsch-Marte, *J. Microscopy* **230**, 134 (2008).
6. G. Situ, G. Pedrini, and W. Osten, *J. Opt. Soc. Am. A* **26**, 1788 (2009).
7. T. Yi, J. Dong, X. Zhu, G. Yang, and S. Liu, *Acta Opt. Sin.* (in Chinese) **30**, 753 (2010).
8. A. Jesacher, S. Fürhapter, S. Bernet, and M. Ritsch-Marte, *Phys. Rev. Lett.* **94**, 233902 (2005).
9. X.-C. Yuan, N. Zhang, S. H. Tao, J. Bu, and J. Lin, *Appl. Phys. Lett.* **91**, 171116 (2007).
10. G. Situ, M. Warber, G. Pedrini, and W. Osten, *Opt. Commun.* **283**, 1273 (2010).
11. M. V. Berry, *J. Opt. A* **6**, 259 (2004).